*Progress In Electromagnetics Research B, Vol. 99, 41–62, 2023*

# Design of Waveguide Applicators Using a Quarter-Wave Transformer Prototype

**Mykola Zhuk*** **and Jonathan Paradis**

**Abstract**—In this paper, we propose a design methodology for waveguide applicators to maximize microwave power deposition into human tissues. The optimized applicators can be used in the experimental studies of the biological effects of exposure to electromagnetic radiation in the frequency range from 6 GHz to 100 GHz. The design methodology relies on the provision of reflectionless matching of a dissipative waveguide load, achieved by employing a matching network based on a quarter-wave transformer prototype. The prototype is synthesized by knowledge of the voltage standing wave ratio (VSWR) evaluated in the unmatched loaded waveguide. A key difference from the conventional synthesis procedure is that in our design approach, the characteristic impedance of the first transformer section is given, and we have to not only determine the characteristic impedances of the remaining sections, but also establish the output load. A solution of this synthesis problem and the process of converting the transformer prototype into a waveguide structure are described. The physical structure can be implemented according to provided sample models of waveguide WR137 applicators employing symmetric inductive or capacitive posts. The matched waveguide applicators are easy to manufacture, and according to the results from computational simulations, they demonstrate superior performance compared to the unmatched waveguides. Limitations of our designs (narrow bandwidth, dependence on the type of tissues encountered, limited potential for miniaturization) are discussed.

## 1. INTRODUCTION

This work describes a simple method of achieving effective transmission of a guided wave into an absorbing load via a lossless matching network. The suggested methodology is applied to the design of waveguide radiofrequency (RF) applicators for depositing microwave energy into human tissues. We concentrated on this class of passive components due to our interest in the experimental study of the biological effects of exposure to RF electromagnetic (EM) radiation in the frequency range from 6 GHz to 100 GHz.

The fast-growing spectrum usage above 6 GHz is driven by the need to meet the demands of existing and emerging mobile communication technologies [3]. This calls for an experimental study of human exposure to microwave energy above 6 GHz from a health risk perspective with the purpose of formulating the science-based limits for such exposures [11] and the verification of the accuracy of relevant theoretical models [9, 17]. The objective of experiments is to determine a relationship among biological responses, health-related physical effects (e.g., a change in tissue temperature), and the characteristics of EM field. A key element of such experiments is the provision of *localized* deposition of microwave energy in biological tissues. In this context, conventional directional antennas have limited usefulness because in the usual, far-field region of antenna operation, the size of the illuminated spot is much larger than the wavelength of radiation [30, Sec. 2.4.3]. A better candidate for this purpose

*Received 19 December 2022, Accepted 28 February 2023, Scheduled 14 March 2023*

* Corresponding author: Mykola Zhuk (mykola.zhuk@canada.ca).

The authors are with the Consumer and Clinical Radiation Protection Bureau, Health Canada, 775 Brookfield Road, A. L. 6302C, Ottawa, Ontario, K1A 1C1, Canada.

is the open-ended waveguide because it can produce irradiated spots with the size of the aperture if it is placed close enough to the skin surface, and suffers lower dissipative loss than coaxial cables or microstrips.

The main concern with waveguide applicators is that incident energy *reflects* on the skin surface. In the microwave hypertermia systems for superficial treatments [12, 26, 10, 5, 23, 32] (which are typically operated at either 434 MHz or 915 MHz), this issue is mitigated by filling the space between the applicator and skin with a matching medium — water — which is circulated through the bolus. However, the method is impractical in the case of present interest because of the unacceptable loss of microwave power in the water. In [34], a fullband coupling of waveguide WR5 to biotissues is realized at THz frequencies using a tapered dielectric rod as a matching structure. In that design, the rod has to be fixed at the center of the waveguide. This feature makes the design challenging mechanically because the transverse size of the rod is smaller than that of the waveguide.

We propose in this paper a method for providing effective transmission of a guided wave power into human tissues by using a lossless impedance-matching network to match the resistance part of the load impedance into the transmission line (TL) impedance. The main concept of our design methodology is to realize the impedance matching by using a *quarter-wave transformer* prototype [22, Sec. 6.02]. The latter is then implemented as a cascade of TL inhomogeneities — obstacles — distributed along the TL.

It is believed that our method may also prove useful in the design of waveguide terminations [31, Sec. 3.7.4], probes for the detection of defects in composite materials [39], antennas for intra-body communications [2], wireless power transfer devices for medical implants [14, 25], and in other applications where there is an impedance mismatch between the transmission line and the load. (The term "impedance" is used here to incorporate reflection coefficient and related notions.)

In the standard synthesis procedure for quarter-wave transformer prototypes [27], the output load is given, and the task at hand is to find the characteristic impedances of all transformer sections. Our needs dictate a different procedure whereby the characteristic impedance of the first section is given, and we have to not only determine the characteristic impedances of the remaining transformer sections, but also establish the output load. This subject is elaborated for the arbitrary order of the prototype presented in Appendix A. The closed-form solution of low-order prototypes is presented in Section 2 and is based on the results of [22, Sec. 6.04].

In the implementation phase, the transformer prototype is converted to a waveguide design by replacing the TL junctions of the transformer prototype with equivalent waveguide networks operating in the $TE_{10}$ mode. Physical foundations for this procedure are well known and described in half-wave filter design literature, e.g., in [37]. An essential component of such a procedure is the determination of the location of requisite reference planes for waveguide discontinuities or obstacles. Appendix B presents an exact and fairly simple solution to this problem in terms of scattering coefficients of obstacles. This solution is simpler than the method of [19], which uses impedance or admittance inverters to characterize the obstacles.

Our design method is described in Section 2. It can synthesize an applicator that is matched to a human body part — even that embedded with an implant, and for any placement configuration of the applicator with respect to the tissue region. For example, the applicator can be stationed in a slanted position at some distance from the skin surface.

The reason for such universality is that the surroundings of the applicator *indirectly* consist in the synthesis procedure. Namely, in order to carry out the design process, all we need to know about the surroundings is the modal reflection coefficient (phase and magnitude) at the operating frequency $f_0$ for the *unmatched* waveguide installed in a fixed position relative to the considered body part. Clearly, this imposes a restriction on how the optimized, matched applicator may be used; it must be applied to the same body part and positioned relative to it the same way the unmatched waveguide was. In the case of a medical implant, however, its frequency response must be non-resonant to ensure a slow variation of the aforementioned reflection coefficient over the considered frequency range.

In this paper, we determine the required reflection coefficient *numerically* using HFSS and a simplified, plane-layered model of human tissues, whereas, alternatively, in practical situations it could be measured *experimentally* with a vector network analyzer using a waveguide test port. Our numerical examples in Section 3 serve to explain the principles of the design method and are limited to the simplest

situation where the applicator is perpendicular to the (locally) flat skin surface, and the waveguide aperture is flush with the latter, thus the analysis of other design examples is left for future research.

Note that EM simulations reported in this paper were carried out by the finite-element method using Ansys HFSS (Ansys Inc., Canonsburg, PA). All other computations were done with Wolfram Mathematica (Wolfram Research, Champaign, IL).

## 2. DESIGN METHOD

This section pertains to the design of matched waveguide applicators that make use of a quarter-wave transformer prototype. Fig. 1 shows an example of such a prototype which is composed of $n$ ($n \geq 1$) TL sections that all have the same electrical length $\theta$ (which changes with frequency $f$), and is terminated with TLs of characteristic impedances $r_G$ on the left and $r_L$ on the right. Otherwise stated, the parameters $r_G$ and $r_L$ may represent the internal resistance of a voltage generator and the load resistance, respectively.

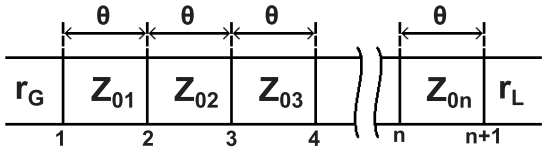


**Figure 1.** A quarter-wave transformer prototype terminated in the source resistance $r_G$ and load resistance $r_L$, and consisting of $n$ TL sections of electrical length $\theta$ and characteristic impedances $Z_{01}, Z_{02}, \ldots, Z_{0n}$ ($\theta = \frac{\pi}{2}$ is the passband center).

We first synthesize a Chebyshev quarter-wave transformer prototype whose insertion loss function and consequent power reflection coefficient will be approximated by the matched waveguide structure. Appendix A presents, in a condensed form, the formulas required to accomplish this task.

As a second, final step, the transformer prototype is implemented in the waveguide structure and is constructed using the two-port networks — waveguide scatterers — that produce the desired scattering matrices. The underlying theory is developed in Appendix B.

**The unmatched structure** represents an air-filled waveguide which propagates the $TE_{10}$ mode and deposits energy into an absorbing load (e.g., living tissues), while the other end consists of the waveguide port launching the EM wave. An example of this concept is illustrated in Fig. 2, where the flanged end of the applicator is sealed by a low-loss dielectric slab (shown as a gray box) inset in a metal cavity (metal is henceforth denoted as yellow). The purpose of the dielectric slab is twofold: a) to provide isolation from environmental conditions and prevent the ingress of moisture into waveguide housings, b) to reduce reflection from the tissue and thus increase the bandwidth of the optimized, *matched* applicator.

If the material inside the body of the slab is air, we arrive at a subsidiary model of a *hollow* open-ended waveguide. The right panel of Fig. 2 visualizes the waveguide's $H$-plane cross section; the operating arrangement whereby the waveguide is perpendicular to and is in direct contact with the flat surface of the body part. The latter is schematically shown as a planar slab composed of four tissue layers. However, our applicator design method can be matched (in principle at least) with a generic composition and geometry of the body part (for example, the latter may contain an implanted receiver, etc.)

To initiate the design process of a matched structure, we assume that we know — either from simulation or measurement, the complex (magnitude and phase) modal reflection coefficient at a given *synchronous* frequency $f_s$ for the *unmatched* waveguide operating into the load. As such, the matched applicator has to be positioned at the same fixed relation determined for the unmatched waveguide. The corresponding voltage standing wave ratio (VSWR) in the unmatched structure is denoted by $V_1'$ and the phase of the reflection coefficient (de-embedded to an appropriate reference plane) by $\theta_{bb}'^{(1)}$. We use this notation in order to emphasize association of this reflection coefficient with the one-port networks $N_1'$ in Fig. 3 and $N'$ in Fig. B2.

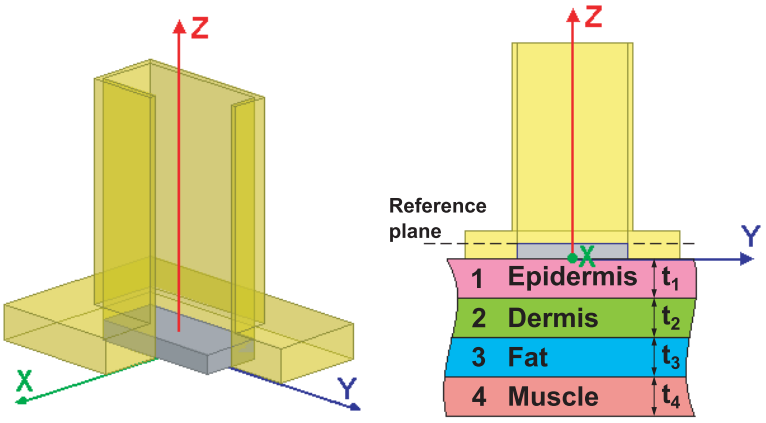


**Figure 2.** Cutaway drawing of the unmatched flanged waveguide showing the inset dielectric slab (gray section) and cross-sectional view of the waveguide and human tissues (numbered 1 to 4). Notice that the pictures are not drawn to scale. In the numerical examples (Section 3), we consider the standard WR137 waveguide with a Teflon slab of thickness 5.08 mm, and two sets of tissue thicknesses; $t_1 = 0.1$ mm, $t_2 = 1.1$ mm, $t_3 = 3.9$ mm, $t_4 = 23$ mm for the forearm and $t_1 = 0.14$ mm, $t_2 = 4.8$ mm, $t_3 = 7.8$ mm, $t_4 = 23$ mm for the anterior thigh. The complex permittivity of tissues at 7 GHz is given in Table 1.

**Table 1.** Parameters of tissues.

| Layer | Tissue | Dielectric constant $\varepsilon'_r$ | Loss factor $\varepsilon''_r$ | Thickness |
|---|---|---|---|---|
| 1 | Epidermis | 27.7 | 8.4 | $t_1$ |
| 2 | Dermis | 35.5 | 12.5 | $t_2$ |
| 3 | Fat | 5.0 | 1.0 | $t_3$ |
| 4 | Muscle | 47.4 | 17.4 | $t_4$ |

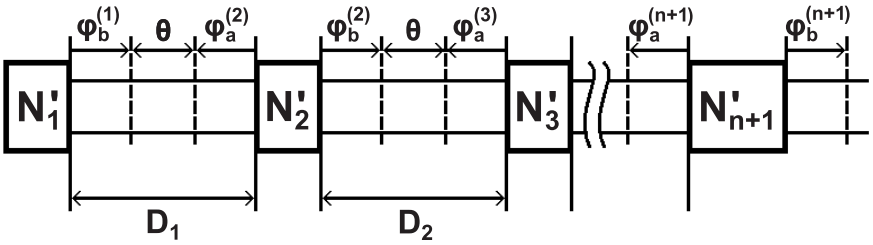


**Figure 3.** Waveguide implementation of the quarter-wave transformer prototype shown in Fig. 1 by means of obstacles $N'_2$, $N'_3$, $N'_{n+1}$ and additional electrical separations $\varphi_b^{(1)}, \varphi_a^{(2)}, \varphi_b^{(2)}, \ldots, \varphi_b^{(n+1)}$, showing the physical lengths $D_1, D_2, \ldots$ of waveguide sections.

The synchronous frequency is understood here as a fixed frequency at which the performances of the matched structure and the transformer prototype coincide — cf. [22, p. 258]. For methodological reasons, it is convenient to keep it unspecified as yet; eventually it will be set to the center frequency $f_0$ of the *desired* passband of the matched structure.

It is assumed that $1 < V'_1 < +\infty$. In the particular case $V'_1 = 1$ the load is reflectionless, and there is no mismatch to be compensated. The case $V'_1 = +\infty$ corresponds to the perfectly reflective load which does not absorb power, and therefore cannot be matched to the waveguide with the help of a lossless network.

The choice of the reference plane for the modal reflection coefficient in the unmatched structure is of secondary importance. The main point here is to simplify formulations of our design approach to facilitate waveguide implementation. We find it convenient to choose the location of the reference planes either on the side of the dielectric slab looking into the waveguide or right at the aperture plane (in the case of a hollow structure). In Fig. 2, the reference plane is signified by a dashed horizontal line.

**The quarter-wave transformer prototype** is treated from a general point of view in Appendix A. The synthesis procedure presented therein is illustrated here in relation to the waveguide realization of a theoretical prototype. We start with specifying the impedance $r_G$ of the input TL, number of sections ($n$), the sign parameter ($\nu$), and either the passband return loss ($RL$) in dB ($RL > 0$) or the passband ripple parameter $\epsilon$ defined by Eq. (A9). Noting here that the higher the value $n$ is, the wider the bandwidth of the transformer is, whereas larger values of $RL$ reduce the bandwidth (although in turn provide better return loss across the passband). The sign parameter $\nu$ is a special kind of variable which by Eq. (A12) may be either 1 or $-1$. For $\nu = 1$ or $\nu = -1$, the impedance levels increase or decrease, respectively, from the first to last sections of the prototype. As shown below, for any $r_G > 0$ and either choice of $\nu$ we get exactly the *same* design for the matched waveguide structure. Therefore, the impedance $r_G$ of the input TL can be set equal to 1 ohm (or whatever positive value), and $\nu$ can be chosen as 1 without affecting the waveguide implementation.

Next, we impose a condition where the individual VSWR $V_{1,req}$ of the first junction in Fig. 1 is *identical* to that of the unmatched waveguide irradiating the human body part: $V_{1,req} = V_1'$. This condition enables us to find the characteristic impedance $Z_{01,req}$ of the first transformer section: $Z_{01,req} = r_G V_{1,req}^{\nu}$.

After that, we diligently follow the recipe of Appendix A; namely, determine from Eq. (A23) the requisite numerical solution $\mu_0$ ($0 < \mu_0 < 1$) for the bandwidth parameter $\mu$, calculate the load resistance $r_{L,req}$, obtain the characteristic impedances $Z_{02,req}, Z_{03,req}, \ldots, Z_{0n,req}$ of the remaining sections, and determine the individual VSWRs $V_{2,req}, V_{3,req}, \ldots, V_{n+1,req}$ of the remaining junctions of the prototype. Note that the symbols $r_L$, $Z_{0k}$, and $V_k$ are used in Appendix A for the respective functions $r_L(n, \epsilon, \mu, \nu)$, $Z_{0k}(n, \epsilon, \mu, \nu)$ and $V_k(n, \epsilon, \mu)$ with an arbitrary $\mu > 0$. We use the subscript $req$ to indicate the values of these functions at $\mu = \mu_0$. As described in Appendix A, the quantity $\mu_0$ and junction VSWRs are the same for $\nu = 1$ and $\nu = -1$.

In the particular case of a one-section prototype ($n = 1$), we obtain, based on the general results of Appendix A, the following explicit expressions:

$$V_{2,req} = V_{1,req}, \tag{1}$$

$$\mu_0 = \frac{2\epsilon}{V_{1,req} - \dfrac{1}{V_{1,req}}}. \tag{2}$$

Closed-form solutions to the classical transformer synthesis problem for $n = 2, 3, 4$ were given in [22, Sec. 6.04]. Suitably adapted to our synthesis procedure, these solutions lead to the following expressions for $n = 2$:

$$V_{2,req} = \frac{r}{V_{1,req}^2}, \tag{3}$$

$$V_{3,req} = V_{1,req}, \tag{4}$$

$$\mu_0 = \frac{\sqrt{2}}{\left[1 + \dfrac{1}{2\epsilon}\left(\sqrt{r} - \dfrac{1}{\sqrt{r}}\right)\right]^{1/2}}, \tag{5}$$

where

$$r = \frac{V_{1,req}^4}{\left(\epsilon + \sqrt{1+\epsilon^2}\right)^2}, \tag{6}$$

and for $n = 3$:

$$V_{2,req} = V_{3,req} = \frac{\sqrt{r}}{V_{1,req}}, \tag{7}$$

$$V_{4,req} = V_{1,req}, \tag{8}$$

where

$$r = 1 + 2\epsilon\mathfrak{T}_3\left(\frac{1}{\mu_0}\right)\left[\sqrt{1+\epsilon^2\mathfrak{T}_3^2\left(\frac{1}{\mu_0}\right)} + \epsilon\mathfrak{T}_3\left(\frac{1}{\mu_0}\right)\right], \tag{9}$$

$\mathfrak{T}_3(x)$ is the 3rd order Chebyshev polynomial of $x$, and $\mu_0$ is the real positive root on the interval $(0, 1)$ of the following equation:

$$2\epsilon\mathfrak{T}_3\left(\frac{1}{\mu_0}\right) = \left(V_{1,req} - \frac{1}{V_{1,req}} - \frac{3\epsilon}{\mu_0}\right)\left(V_{1,req}^2 + \frac{1}{V_{1,req}^2}\right) + \sqrt{1+\left(V_{1,req} - \frac{1}{V_{1,req}} - \frac{3\epsilon}{\mu_0}\right)^2}\left(V_{1,req}^2 - \frac{1}{V_{1,req}^2}\right). \tag{10}$$

We skip solving for $n = 4$ from [22, Eq. (6.04.4)] for the sake of brevity, since we do not consider it among our numerical examples. To adapt Eq. (6.04.4) to the context of the present paper, one has to rewrite it by replacing $R$ everywhere (we are using here the notation of [22]) including the quantities $A^2$ and $B$, with our function $r(n, \epsilon, \mu, \nu)$ from (A15) taken at $n = 4$, $\mu = \mu_0$, $\nu = 1$. Then† the first line of [22, Eq. (6.04.4)] converts into an equation for $\mu_0$, and the two subsequent expressions give $V_2$ and $V_3$ (note that $V_4 = V_2$ and $V_5 = V_1$).

**The matched applicator**. In the final implementation step, we use the unmatched waveguide structure as a starting point and realize the waveguide matching network by transforming each section of the prototype to a waveguide section, replacing each TL junction by an appropriate waveguide obstacle. To work out the waveguide-based design, all we need to know about the prototype is the VSWR at each junction. Unless explicitly stated, the presentation below refers to a fixed synchronous frequency $f_s$ within the single-mode frequency range of the waveguide — thus, the prototype and the matched waveguide applicator can be made equivalent (in the sense of Appendix B) at *any* such frequency and *any* value of $\theta = \theta(f_s)$.

In the schematic of the matched structure network (Fig. 3), $N_1'$ represents an unmatched structure. By choosing the synthesis parameter $\mu_0$ to satisfy Eq. (A23), we have already ensured that junction 1 of the prototype produces the same VSWR ($V_{1,req}$) as that of ($V_1'$) appertaining to the unmatched structure. Junction 1 and the unmatched structure play, respectively, the role of networks $N$ and $N'$ in Fig. B2. Now we select the electrical distance $\varphi_b^{(1)}$ along the waveguide in accordance with Eq. (B26), and set the phase of the reflection coefficient (B25) for the arising one-port $N_1''$ (network $N''$ as shown in the nomenclature of subsection B3, Appendix B) equal to the phase of the reflection coefficient of junction 1 (by which we mean the reflection coefficient (B27) when a stimulus is applied from the TL of characteristic impedance $Z_{01}$). One can easily verify that such a choice of $\varphi_b^{(1)}$ makes the reactance part of the input impedance of network $N_1''$ vanish. In other words, the absorbing load, in conjunction with the Teflon slab (as seen through the waveguide section of electrical length $\varphi_b^{(1)}$), represents a pure resistance.

Next, for each junction $k = 2, 3, 4, \ldots, n+1$ in Fig. 1, we design an appropriate obstacle — the *two-port* lossless reciprocal waveguide network $N_k'$ (shown in Fig. 3) that produces the same individual VSWR $V_k'$ as that of ($V_{k,req}$) due to the network component $N_k$ — the junction $k$ of the prototype. The equivalence principle involving these networks is described in subsections B1 and B2 of Appendix B. Various quantities pertaining to networks $N$, $N'$, and $N''$ in that analysis will be accompanied here by the label $k$. For example, $\theta_{aa}^{\prime(k)}$, $\theta_{bb}^{\prime(k)}$, $\theta_{ab}^{\prime(k)}$ and $\varphi_a^{(k)}$, $\varphi_b^{(k)}$ are the phases $\theta_{aa}'$, $\theta_{bb}'$, $\theta_{ab}'$, and electrical distances $\varphi_a$, $\varphi_b$ that appear in Eqs. (B5), (B16)–(B19) are defined here for the network $N_k'$ in exactly

† The subscript *req* has to be added to the $V_k$ of [22, Eq. (6.04.4)] to conform to the notation of this paper.

the same way they are defined for the network $N'$ in Fig. B1. By selecting $\varphi_a^{(k)}$, $\varphi_b^{(k)}$ in accordance with Eqs. (B16)–(B19), each obstacle is transformed into a waveguide network $N_k''$ that has the same scattering matrix $\underline{\underline{S}}_k''$ (B9) as the corresponding junction $k$ of the prototype — see Eq. (B20). Note that the waveguide section of electrical length $\varphi_b^{(n+1)}$ on the right has no practical role because it is absorbed into the input port of the applicator.

Once all obstacles and electrical spacings have been determined, it is easy to see that the reflection coefficient of the waveguide applicator for the frequency $f_s$ at the reference plane (defined by the electrical distance $\varphi_b^{(n+1)}$ in Fig. 3) coincides with that of the transformer prototype (using the sections of electrical length $\theta$) at junction $n+1$ in Fig. 1.

The above method of converting a prototype network into a waveguide network to design a direct-coupled waveguide filter is well known (see [37]). We adapted this method in a way that simplifies the application of the results of Appendix B, where the location of the auxiliary reference planes is given directly in terms of the scattering coefficients of obstacles, rather than the lumped-constant approximations of obstacles [37] or impedance/admittance inverters [19].

The physical lengths $D_k$ of the waveguide sections can be found as follows [37]. Let us consider a length $D_k$ of the waveguide between obstacles $N_k'$ and $N_{k+1}'$ $(k = 1, 2, \ldots, n)$ as shown in Fig. 3. The actual electrical length of this waveguide section for the synchronous frequency $f_s$ is $\beta D_k$, where $\beta$ is the modal propagation constant at $f = f_s$. On the other hand, according to Fig. 3, the required electrical length of the same waveguide section at the synchronous frequency is $\varphi_b^{(k)} + \theta + \varphi_a^{(k+1)}$, where all quantities are evaluated at $f = f_s$. The actual and required electrical lengths should be the same, hence the physical length $D_k$ of the waveguide section is found to be:

$$D_k = \frac{1}{\beta}\left(\varphi_b^{(k)} + \theta + \varphi_a^{(k+1)}\right) \quad (k = 1, 2, 3, \ldots, n) \tag{11}$$

As shown in Appendix B, for $k = 1, 2, 3, \ldots, n+1$ there is an infinite number of positions for the auxiliary reference planes which define the equivalent networks $N_k''$. In order to ensure a wider frequency range of operation of the applicator, it is recommended [19] to choose the (positive or negative) electrical lengths $\varphi_b^{(k)}, \varphi_a^{(k+1)}$ used in Eq. (11) such that the absolute value of $\varphi_b^{(k)} + \varphi_a^{(k+1)}$ is the smallest.

Now we arrive at the final point; after substitution of expressions (B19), (B26) for $\varphi_b^{(k)}$ and (B16) for $\varphi_a^{(k+1)}$ into Eq. (11) and taking Eqs. (B21)–(B22), (B28) into account, we see that the expressions for $D_k$ assume the same form for both $\nu = 1$ and $\nu = -1$, viz:

$$D_k = \frac{1}{\beta}\left[\frac{\theta_{bb}'^{(k)} + \theta_{aa}'^{(k+1)}}{2} + \theta - \frac{\pi}{2} + \pi\left(n_b^{(k)} + n_a^{(k+1)}\right)\right] \quad (k = 1, 2, 3, \ldots, n) \tag{12}$$

where $\theta_{bb}'^{(k)}$, $\theta_{aa}'^{(k+1)}$ and $n_b^{(k)}$, $n_a^{(k+1)}$ are the phases $\theta_{bb}'$, $\theta_{aa}'$ and the constants $n_b$, $n_a$ from Appendix B specialized to the waveguide networks $N_k''$, $N_{k+1}''$, respectively. The quantities $\theta_{bb}'^{(k)}$, $\theta_{aa}'^{(k+1)}$ on the right hand side of Eq. (12) are evaluated at synchronous frequency $f_s$. It can be easily seen from (12) that the physical lengths $D_k$ and, consequently, the physical realization of the matched waveguide applicator do not depend upon whether we have used the prototype transformer with the increasing ($\nu = 1$) or decreasing ($\nu = -1$) impedance levels.

As well known, a sensible choice for the synchronous frequency $f_s$ is to set it to the center (midband) frequency $f_0$ of the *desired* passband of the matched waveguide structure and postulate that the electrical length $\theta = \theta(f_0)$ of each transformer section (Fig. 1) is $\pi/2$ at this frequency. The physical lengths of waveguide sections for such a choice of $f_s$ are given by Eqs. (11), (12) where $\theta$ should be replaced by $\pi/2$, and $\beta$ by $\beta_0$ — the waveguide propagation constant at frequency $f_0$. As seen from (12), the quantity $2\beta_0 D_k - \theta_{bb}'^{(k)} - \theta_{aa}'^{(k+1)}$ in the present case is an integer multiple of $2\pi$. This coincides with the condition of constructive interference for the guided wave in the $k$-th waveguide section and suggests an alternative purpose of the matched structure as a waveguide bandpass filter [22, Sec. 6.03]. However, we do not pursue this avenue in the present paper except to note that the applicators described in the next section can be tuned by using the well-known technique for such filters.

Namely, with regards to the applicator shown in Fig. 4(b), if the lengths $D_1, D_2, D_3$ of waveguide sections and the distances $s_2, s_3, s_4$ between the posts in each row are made slightly shorter than required, the frequency response of the applicator can be adjusted by pushing short screws through the broad wall into the waveguide. Then the center frequency can be controlled by a tuning screw in the middle of each waveguide section, and the return loss across passband — achieved by a coupling screw placed between the posts of each of rows $2', 3', 4'$.

A useful performance parameter of an applicator is the fractional bandwidths at a specified level of return loss. This parameter is defined by the formula

$$w,\ \% = \frac{2\,(f_{\max} - f_{\min})}{f_{\max} + f_{\min}} \cdot 100, \tag{13}$$

where $f_{\max}$ and $f_{\min}$ are the maximal and minimal frequencies within the passband for which the value of return loss assumes the specified value. We use this parameter as the basic comparison metric for the computer-aided designs of matched applicators described below.

## 3. SIMULATION RESULTS

In the numerical examples, we consider the standard WR137 waveguide (nominal frequency range 5.85 GHz to 8.20 GHz) which has inner dimensions of $a = 34.85$ mm, $b = 15.80$ mm, and the dielectric slab inserted therein has transverse dimensions of $a \times b$ and a thickness of 5.08 mm. The material of the slab is lossless Teflon (relative dielectric constant 2.08), and all metal parts are assumed to be perfect electric conductors (PECs). Fig. 4 schematically illustrates the features of the proposed waveguide applicators; the partial-height capacitive post (left panel) or inductive full height posts (right panel). These applicators are attached to the tissues in the same way as the unmatched waveguide in the right panel of Fig. 2. The matched applicators are classified as Type A (matched to the human forearm) or Type T (matched to the anterior thigh). For brevity, we below refer to these body parts as the arm and the thigh. These two cases are chosen because they are different with regard to the thickness of tissue layers. Further research on assessing typical human tissues composition and EM properties across body parts is warranted, since it could further highlight the capacities and limitations of matching.

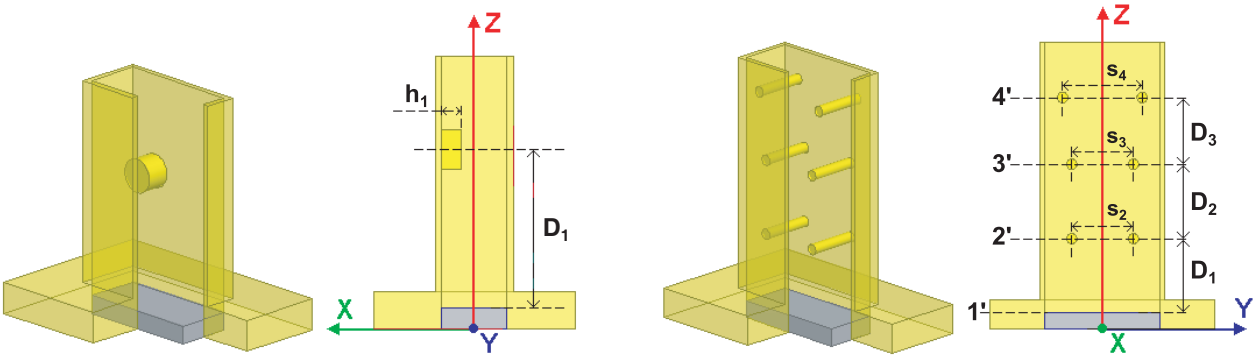


**Figure 4.** Cutaway drawing and cross-sectional view of waveguide WR137 applicators of Type A (matched to the human forearm) or Type T (matched to the anterior thigh) using a Teflon slab (the gray box) of thickness 5.08 mm: (a) 1-section applicator with the symmetric capacitive post of diameter 9.525 mm: $D_1 = 25.91$ mm, $h_1 = 7.85$ mm for Type A, and $D_1 = 25.50$ mm, $h_1 = 6.78$ mm for Type T, (b) 3-section applicator with the symmetric inductive posts of diameter 3.175 mm (the dimensions $s_2$, $s_3$, $s_4$ and $D_1$, $D_2$, $D_3$ are given in Table 2).

The tissue model considered consists of the four planar layers listed in Table 1. The complex relative permittivity $\varepsilon_{cr}$ of tissues is defined as $\varepsilon_{cr} = \varepsilon'_r - j\varepsilon''_r$. The dielectric constant $\varepsilon'_r$ and loss factor $\varepsilon''_r$ are assumed to be independent of frequency and are chosen based on the EM properties

of respective tissues at 7 GHz measured over a wide frequency range in [28, 29]. The thicknesses of layers will vary over different body regions and among individuals. We considered two sets of tissue thicknesses; $t_1 = 0.1\,\text{mm}$, $t_2 = 1.1\,\text{mm}$, $t_3 = 3.9\,\text{mm}$, $t_4 = 23\,\text{mm}$ for the arm and $t_1 = 0.14\,\text{mm}$, $t_2 = 4.8\,\text{mm}$, $t_3 = 7.8\,\text{mm}$, $t_4 = 23\,\text{mm}$ for the thigh for which the dimensions $t_1$, $t_2$, and $t_3$ are in accordance with previous studies [16, 28, 29].

The value of parameter $t_4$ is smaller than the typical thickness of the muscle layer in the considered body parts and is chosen so in order to reduce the size of the computational domain, while not affecting the computed values of the quantities of interest. Justified by the highly lossy nature of tissues, these considerations also form the basis for limiting the size of the tissue sample in the $x$ and $y$ directions, and applying a PEC boundary to all outer faces of the solution domain, including the bottom surface of Layer 4 and the segment of the top boundary $z = 0$ of Layer 1 outside of the waveguide flange. The latter amounts to an assumption of an *infinite flange* and is of purely technical nature; it frees us from the need to simulate the radiation away from the tissue into the upper halfspace. Obviously, this approximation works well when the flange is sufficiently large. Note that by limiting the computational domain to the tissues within the PEC boundary, we make the waveguide wall thickness and the actual flange size irrelevant for simulations.

The important point is that the microwave energy needs to be transitioned from a coaxial to a waveguide interface (we owe this remark to one of the anonymous reviewers). For the frequency range of interest, advances in the design theory [4, 20] and technological procedures have essentially eliminated the problem of such transitions, as far as our designs are concerned. All major companies specializing in manufacturing passive microwave components offer several models of high-quality coax-to-waveguide adapters for frequencies up to 100 GHz. Such adapters provide effective transmission of microwave energy from the coaxial cable to the waveguide, thus allowing us to use the *wave port* to excite the waveguides in our HFSS models.

In Fig. 4, the single-mode wave port is assigned on the top end of the waveguides. The complex modal reflection coefficient referring to this port is denoted by $S_{11}$; its magnitude (in dB) as function of frequency $f$ is plotted in Figs. 5–7. (We caution the reader that the symbol $S_{11}$ has a different meaning in Appendix A.)

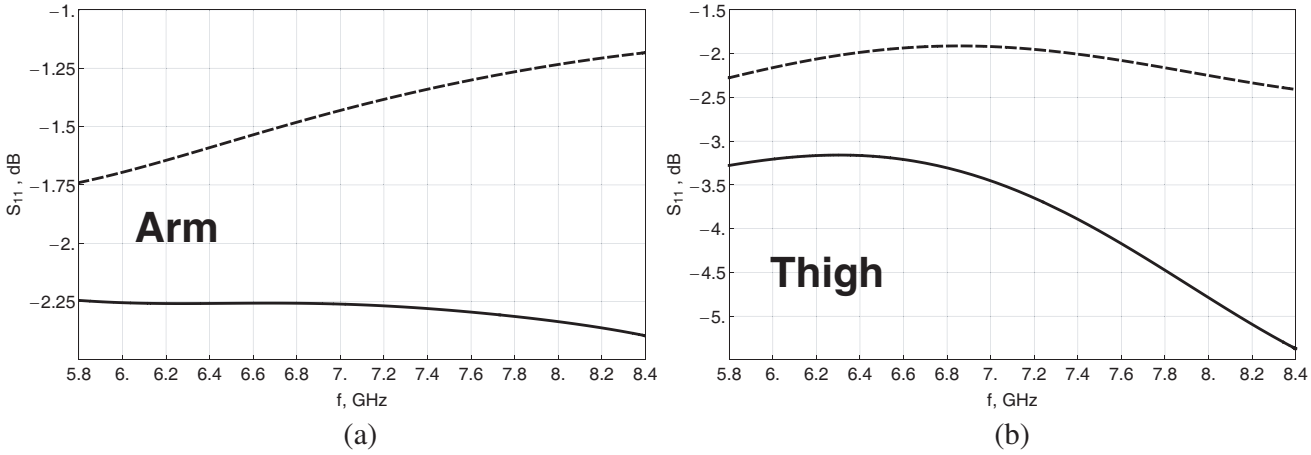


**Figure 5.** Reflection coefficient, in dB, for unmatched waveguide WR137 structures: the waveguide with the Teflon slab (solid line) and the hollow open-ended waveguide (dashed line) in contact with (a) the arm and (b) the thigh.

Figure 5 shows the computed reflection coefficient for the waveguides from Fig. 2 when these waveguides are attached to the arm or thigh, respectively.

The dimensions for the one-section matched applicator in Fig. 4(a) with a symmetric capacitive post (diameter 9.525 mm, which is equivalent to a screw # 3/8) are as follows: $D_1 = 25.91\,\text{mm}$, $h_1 = 7.85\,\text{mm}$ for Type A, and $D_1 = 25.50\,\text{mm}$, $h_1 = 6.78\,\text{mm}$ for Type T. The dimensions for the $n$-section matched applicators in Fig. 4(b) using symmetric inductive posts of diameter 3.175 mm are given in Table 2

**Table 2.** Dimensions for matched waveguide applicators from Fig. 4(b) with symmetric inductive posts of diameter 3.175 mm.

| Number of sections | Dimensions, mm, for Type A applicators | | | | | | Dimensions, mm, for Type T applicators | | | | | |
|---|---|---|---|---|---|---|---|---|---|---|---|---|
| | $s_2$ | $s_3$ | $s_4$ | $D_1$ | $D_2$ | $D_3$ | $s_2$ | $s_3$ | $s_4$ | $D_1$ | $D_2$ | $D_3$ |
| $n = 1$ | 19.71 | n/a | n/a | 19.25 | n/a | n/a | 21.18 | n/a | n/a | 17.63 | n/a | n/a |
| $n = 2$ | 14.33 | 19.71 | n/a | 21.29 | 23.93 | n/a | 16.46 | 21.18 | n/a | 19.66 | 22.58 | n/a |
| $n = 3$ | 12.85 | 12.85 | 19.71 | 21.62 | 26.59 | 24.26 | 15.14 | 15.14 | 21.18 | 20.09 | 25.50 | 23.01 |

(note the jump in notation on the just cited figure, and there is no such quantity as $s_1$).

The simulated performance of matched applicators is shown in Figs. 6 and 7. The curves labeled as $n = 1'$ refer to a single section applicator constructed with capacitive posts, and $n = 1, 2, 3$ — to the $n$-section applicators with inductive posts.

The results in Fig. 6 are for the applicators of Type A: the left and right panels correspond to the situations where the applicators are attached to the arm and thigh tissues, respectively. Fig. 7 presents the results for the applicators of Type T when they are attached to the thigh (left panel) and arm (right panel) tissues, respectively.

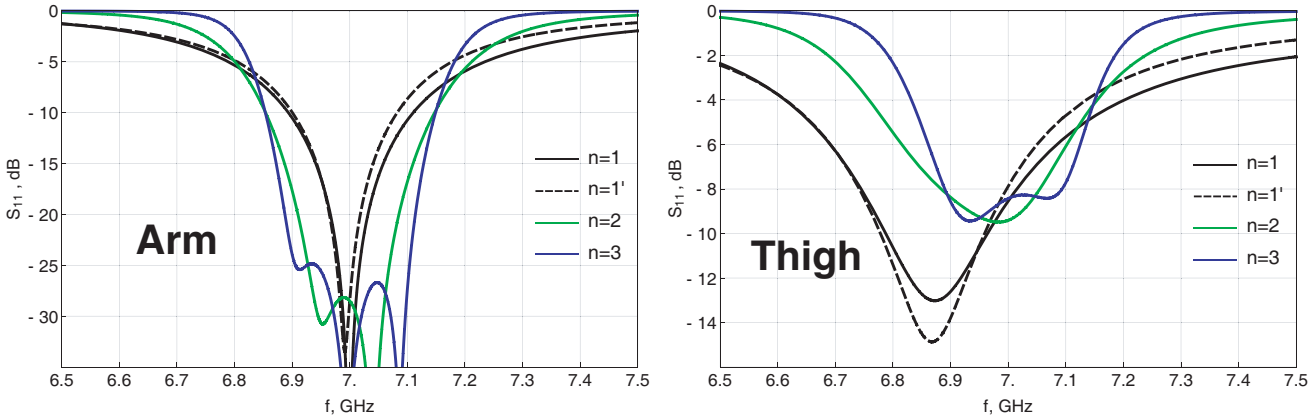


**Figure 6.** Reflection coefficient, in dB, for the matched waveguide WR137 applicator of Type A when it is attached to the (a) arm or (b) thigh tissues. The curves labeled as $n = 1'$ refer to a single-section applicator with the symmetric capacitive post of diameter 9.525 mm described in Fig. 4(a), and $n = 1, 2, 3$ — to the $n$-section applicators with inductive posts of diameter 3.175 mm shown in Fig. 4(b) and characterized in Table 2.

For the purposes of this article, we define the power efficiency $e$ of a given applicator as the worst-case percentage of the incident power that gets delivered to the tissues at 7 GHz. By the term "worst-case" we mean the lowest percentage result of comparison of the applicator performance when attached to either the arm or the thigh. The percentage values of this parameter are summarized in Table 3.

As visible from the plots of Figs. 6 and 7 and results of Table 3, if an applicator is optimized for one type of tissue, but applied to a different type of tissue, the applicator's performance is degraded, yet always exceeds the performance of unmatched waveguides. In the case of single-section applicators using the inductive ($n = 1$) or capacitive ($n = 1'$) posts, we cannot give preference to either of the two designs because they have very similar plots of return loss as a function of frequency. It can also be seen that the bandwidth increases if one increases $n$. The observed return loss across the passband is significantly lower than the value $RL = 30$ dB used in synthesizing the transformer prototype (see

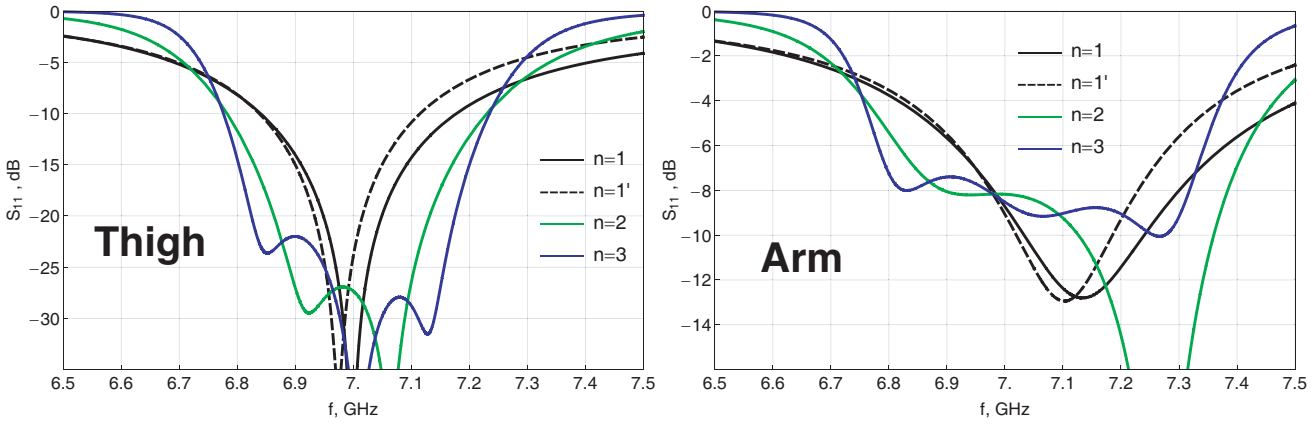


**Figure 7.** Reflection coefficient, in dB, for the matched waveguide WR137 applicator of Type T when it is attached to the (a) thigh or (b) arm tissues. The curves labeled as $n = 1'$ refer to a single-section applicator with the symmetric capacitive post of diameter 9.525 mm described in Fig. 4(a), and $n = 1, 2, 3$ — to the $n$-section applicators with inductive posts of diameter 3.175 mm shown in Fig. 4(b) and characterized in Table 2.

**Table 3.** Efficiency of the unmatched waveguides and matched applicators in terms of percentage of incident power absorbed into tissues of the arm or thigh.

| Efficiency | Unmatched waveguides | | Type A applicators | | | | Type T applicators | | | |
|---|---|---|---|---|---|---|---|---|---|---|
| | Hollow | Teflon slab | $n = 1'$ | $n = 1$ | $n = 2$ | $n = 3$ | $n = 1'$ | $n = 1$ | $n = 2$ | $n = 3$ |
| $e$, % | 28 | 40 | 84 | 86 | 89 | 86 | 88 | 87 | 85 | 86 |

subsection A8 of Appendix A).

Table 4 gives the fractional bandwidth $w$ from Eq. (13) for the matched applicators at a specified level of return loss. The bandwidth values have been extracted from the curves in Figs. 6–7 at the following levels of return loss: 30 dB ($w_{30}$), 21 dB ($w_{21}$), and 6 dB ($w_6$).

Notably, the bandwidths in Table 4 are very different from the performance of the idealized transformer prototypes of Appendix A, with the waveguide devices having a much narrower passband. The bandwidth contraction is a well-known phenomenon which is attributed to the frequency dependence of the scattering coefficients of the obstacles (posts with the short lengths of waveguides attached) [37] in our designs, and of the complex reflection coefficient from the load. We do not analyze this matter in the present paper.

**Table 4.** Matched applicators in terms of fractional bandwidth (from Figs. 6, 7), for return loss levels of 6, 21 and 30 dB.

| Curve | Fig. 6(a) | | | Fig. 6(b) | Fig. 7(a) | | | Fig. 7(b) |
|---|---|---|---|---|---|---|---|---|
| | $w_{30}$, % | $w_{21}$, % | $w_6$,% | $w_6$, % | $w_{30}$, % | $w_{21}$, % | $w_6$, % | $w_6$, % |
| $1'$ | 0.18 | 0.68 | 4.5 | 5.2 | 0.34 | 1.1 | 7.0 | 5.2 |
| 1 | 0.29 | 0.83 | 5.4 | 5.7 | 0.45 | 1.3 | 8.5 | 6.5 |
| 2 | 1.6 | 2.4 | 5.4 | 4.1 | 0.86 | 3.7 | 8.3 | 8.4 |
| 3 | 1.8 | 3.2 | 4.9 | 3.8 | 1.0 | 4.9 | 7.5 | 8.0 |

## 4. DISCUSSION

We proposed in this paper a novel approach for providing effective transmission of a guided wave power into an absorbing load. This approach is based on the concept of impedance matching via a quarter-wave transformer prototype. Realization of this concept requires the solution of a non-conventional synthesis problem which has been solved by modifying the well-known procedure of [27]. The closed-form solution to the synthesis problem is described herein for prototypes of degree $n = 1, 2, 3, 4$. Based on this design method, we developed the designs of efficient waveguide WR137 applicators for depositing microwave energy into human tissues. They can be used in the experimental research of possible health effects arising from RF exposure in the frequency range above 6 GHz.

The feasibility of our designs was validated via computer simulation using HFSS. The suggested applicators are easy to manufacture and tune because they have the same mechanical structure as conventional waveguide bandpass filters [22, Sec. 6.03], and therefore, established manufacturing methods and procedures can be used for their manufacturing [8] and tuning [7, 24].

One important disadvantage of our designs is their *narrow bandwidth* (albeit biomedical applicators presumably very seldom require a broad passband). The two main reasons for this are the significant impedance mismatch of the load, which leads to narrowband transformer prototypes, and the frequency dependence of scattering properties of the networks that have been used as the substitute for the ideal transformer junctions. The first factor is potentially mitigated by placing an optimally stratified high permittivity slab at the aperture of the waveguide instead of the homogeneous Teflon slab used in our designs. The second factor can be dealt with by using obstacles such that the actual length of waveguide sections is close to a quarter wave. This will eliminate the frequency dispersion associated with the additional waveguide lengths currently present in our designs.

Next, the efficiency of a matched applicator is *degraded* if it is applied to tissue structures other than those the applicator is optimized to interact with (nonetheless, increased efficiency is observed over unmatched waveguides). In our opinion, the most efficient (albeit complicated) way to overcome this limitation is to tune the applicator to a specific tissue structure using a fully automated robotic system similar to those described in [38] for microwave filters and multiplexers. Alternatively, the effect of tissue parameters on the applicator performance can be reduced if one uses a more sophisticated synthesis procedure for the transformer prototype, whereby the latter is optimized to provide a match for a *range* of input terminations. This can be achieved via numerical optimization using conventional transformer prototypes as an initial approximation. Note that this suggestion may diminish passband return loss in favor of a decreased sensitivity to tissue parameters for a wider range of tissue structures.

Our approach does not lend well to realizing a *compact* applicator because the length of waveguide sections is related to the guided wavelength. This problem might be mitigated by using waveguide obstacles (see, e.g., [33]) such that the sum $\varphi_b^{(k)} + \varphi_a^{(k+1)}$ of electrical lengths in Eq. (11) associated with any two consecutive obstacles is negative but still smaller by absolute value than $\theta$. Alternatively, metamaterials [15] are known to facilitate miniaturization of passive microwave components (antennas, filters) [32, 1, 13]. A tradeoff of smaller size however is an expected bandwidth reduction.

Note that the aforementioned suggestions must be investigated by further research.

## ACKNOWLEDGMENT

The authors would like to thank Eric Lemay for valuable improvements of the text. Insightful reviews of this paper were gratefully received from Abdel Alzahed, Narine Martel and Robert Stainforth. We thank the anonymous reviewers for their important comments and suggestions.

## APPENDIX A. SYNTHESIS OF QUARTER-WAVE TRANSFORMER PROTOTYPE WITH PRESCRIBED CHARACTERISTIC IMPEDANCE OF THE FIRST SECTION

**A1.** The canonical problem of synthesizing quarter-wave transformer prototypes is described in [22, Ch. 6]. Given the values of the source and load resistances, fractional bandwidth, and order $n$ of the transformer, it is required to determine the passband return loss and characteristic impedances of the $n$ transformer sections. As a minor variation of this problem, the passband return loss is given, and the

fractional bandwidth is a parameter to be determined. A complete solution to this problem was derived in [27].

The synthesis problem behind the design of matched loads and applicators described in the main body of the paper is different from the preceding formulation. Namely, we are given the source resistance $r_G$, passband return loss $RL$, and order $n$ of the transformer, as well as the characteristic impedance $Z_{01,req}$ of the first section, and it is required to determine the characteristic impedances

$$Z_{02,req},\, Z_{03,req},\, \ldots,\, Z_{0n,req} \tag{A1}$$

of the remaining $n-1$ sections and load resistance $r_{L,req}$. It is assumed that $r_G, Z_{01,req} > 0$ and $r_G \neq Z_{01,req}$.

Our solution procedure is composed of the following four steps:

*First,* calculate the ripple parameter $\epsilon$ from Eq. (A9), and determine the sign parameter $\nu$:

$$\nu = \begin{cases} 1 & (Z_{01,req} > r_G) \\ -1 & (Z_{01,req} < r_G) \end{cases} \tag{A2}$$

The parameter $\nu$ defines whether the characteristic impedances of the transformer sections will make an increasing ($\nu = 1$) or decreasing ($\nu = -1$) sequence.

*Second,* find the bandwidth parameter $\mu = \mu_0$ ($0 < \mu_0 < 1$) numerically as the solution to Eq. (A23) which requires that the function $Z_{01}(n, \epsilon, \mu, \nu)$ takes the prescribed value $Z_{01,req}$. Alternatively, $\mu_0$ can be found from Eq. (A24) which demands that the function $V_1(n, \epsilon, \mu)$ takes the known value $V_{1,req}$, where

$$V_{1,req} = \left( \frac{Z_{01,req}}{r_G} \right)^{\nu} \tag{A3}$$

is the VSWR of junction 1 of the prototype transformer (known value). Note that the solution $\mu_0$ depends upon the parameters $n, \epsilon$ and is the same for both $\nu = 1$ and $\nu = -1$.

*Third,* find the corresponding load resistance $r_{L,req}$ from $r_L(n, \epsilon, \mu, \nu)$ by plugging the value $\mu = \mu_0$ into Eqs. (A14), (A15).

*Finally,* determine the characteristic impedances (A1) of the sections $k = 2, 3, 4, \ldots, n$ of the transformer. This can be done in two ways:

First by evaluating the corresponding functions $Z_{0k} = Z_{0k}(n, \epsilon, \mu, \nu)$ at $\mu = \mu_0$. To calculate the latter functions, we developed a variation of the well-known extraction algorithm [18], combined with the transformation [21] of the synthesis variable. This is a comprehensive but technically complicated approach.

Second, from a practical point of view, if a software tool for the conventional synthesis of the quarter-wave $TEM$-line stepped-impedance transformers is available, it is convenient to use the following workaround: by Eq. (A8) and compute the parameter $w_{q0}$ ($0 < w_{q0} < 2$) as

$$w_{q0} = \frac{4}{\pi} \arcsin \mu_0 \tag{A4}$$

(for $TEM$-line transformers, $w_{q0}$ is the fractional passband width between points of the same return loss $RL$ in the *frequency* domain), and then use the software tool to synthesize the characteristic impedances of all transformer sections from knowledge of $n$, source ($r_G$) and load ($r_{L,req}$) resistances, and $w_{q0}$. By doing so, one will, as a by-product, recover the prescribed characteristic impedance of the first section $Z_{01,req}$ and the passband return loss $RL$.

For designing the waveguide matching circuits discussed in Section 3, we need to know the individual VSWRs $V_{k,req}$ for all junctions ($k = 1, 2, 3, \ldots, n+1$) of the transformer prototype. These VSWRs are determined by substituting $\mu = \mu_0$ into relations (A19). For $n = 1, 2, 3$, and 4, it is more advantageous to use the explicit formulas described in Section 2; they are a slight modification of the well-known results obtained in [22, Sec. 6.04].

We shall now derive the basic relations that are necessary for implementing the outlined solution. Further details on the mathematics can be found in References [27, 18].

**A2.** The Chebyshev insertion loss function $P(\theta)$ and associated power reflection coefficient $|S_{11}(\theta)|^2$ are described by the formulas [27, 22, Sec. 6.02]

$$P(\theta) = 1 + \epsilon^2 \mathfrak{T}_n^2(\Omega), \tag{A5}$$

$$|S_{11}(\theta)|^2 = \frac{P(\theta) - 1}{P(\theta)}, \tag{A6}$$

with $\Omega = \frac{\cos\theta}{\mu}$, $\theta$ being the electrical length of a distributed-line section and $\mathfrak{T}_n(\Omega)$ the Chebyshev polynomial (of the first kind) of degree $n$: $\mathfrak{T}_n(\Omega) = \cos(n \arccos \Omega)$. For the quarter-wave transformer, the passband is centered at $\theta = \pi/2$ and is defined as the range

$$\frac{\pi}{2}\left(1 - \frac{w_q}{2}\right) \le \theta \le \frac{\pi}{2}\left(1 + \frac{w_q}{2}\right), \tag{A7}$$

where $w_q$ is the fractional bandwidth of the transformer ($0 < w_q < 2$). The bandwidth parameter $\mu$ is defined as

$$\mu = \sin\frac{\pi w_q}{4}, \tag{A8}$$

and the passband ripple parameter $\epsilon$ ($\epsilon > 0$) is determined from the worst-case return loss $RL$, dB, ($RL > 0$) over the passband:

$$\epsilon = \frac{1}{\sqrt{10^{RL/10} - 1}}, \tag{A9}$$

where typically $RL \gg 1$. Thus, in real-life applications of the transformer prototype we have $0 < \epsilon \ll 1$ and $0 < \mu < 1$. Below, it is computationally convenient to view $\epsilon$ and $\mu$ as arbitrary positive quantities: $0 < \epsilon, \mu < +\infty$. To minimize notation, indication of $n$, $\epsilon$, $\mu$ as the parameters is suppressed in $P$, $|S_{11}|^2$, and subsequent functions.

Following [27], we apply the concept of the Chebyshev response (A5), (A6) to an ideal quarter-wave transformer of Fig. 1 which consists of $n$ ($n \ge 1$) uniform lossless distributed-line sections, each of electrical length $\theta$, terminated in TLs of characteristic impedance $r_G$ and $r_L$ at Ports 1 and 2, respectively. (Alternatively, the parameters $r_G$ and $r_L$ can be interpreted as the generator and load resistances.) The sections are numbered in order from 1 to $n$, starting with the first section which looks into Port 1.

**A3.** The complex reflection coefficient $\Gamma(p)$ at Port 1 is obtained [27] as a real rational function of complex variable $p$ that is *regular* in the halfplane $\mathrm{Re}\, p \ge 0$ and satisfies the following equation on the imaginary axis:

$$|S_{11}(\theta)|^2 = \Gamma(p)\Gamma(-p), \quad (p = -j\cot\theta, \quad 0 < \theta < \pi) \tag{A10}$$

The solution for $\Gamma(p)$ is not unique, due to the sign ambiguity and similarly so for $\mu\cos\frac{\pi}{2n} > 1$, due to the arbitrary choice of the distribution of the zeros of the product $\Gamma(p)\Gamma(-p)$ between the open left and right halves of the complex $p$ plane. We choose the solution to this problem the way it is done in [27]. By Eqs. (A6) and (A10), the limit of $\Gamma(p)$ as $p \to \infty$ is given by

$$\Gamma(\infty) = \frac{\nu \mathfrak{T}_n\left(\frac{1}{\mu}\right)}{\sqrt{\frac{1}{\epsilon^2} + \mathfrak{T}_n^2\left(\frac{1}{\mu}\right)}}, \tag{A11}$$

where $\nu$ is the sign parameter:

$$\nu = \pm 1. \tag{A12}$$

Note that the complete list of arguments of the function $\Gamma$ includes $n, \epsilon, \mu, \nu$ and $p$: $\Gamma(p) = \Gamma(n, \epsilon, \mu, \nu, p)$.

**A4.** There is an additional requirement [27] on $\Gamma(p)$ to be satisfied, viz.

$$\Gamma(\infty) = \frac{r_G - r_L}{r_G + r_L}. \tag{A13}$$

We then solve Eqs. (A13) and (A11) for the load resistance $r_L = r_L(n, \epsilon, \mu, \nu)$, and obtain

$$r_L = r_G\, r, \tag{A14}$$

where the function $r = r(n, \epsilon, \mu, \nu)$ is defined by

$$r(n, \epsilon, \mu, \nu) = \left[ \sqrt{1 + \epsilon^2 \mathfrak{T}_n^2 \left( \frac{1}{\mu} \right)} + \epsilon \nu \mathfrak{T}_n \left( \frac{1}{\mu} \right) \right]^2 . \tag{A15}$$

**A5.** The driving point impedance $Z_d(p) = Z_d(n, \epsilon, \mu, \nu, p)$ of a one-port whose scattering coefficient relative to the port impedance $r_G$ is $\Gamma(p)$ and given by [27]

$$Z_d(p) = r_G \frac{1 + \Gamma(p)}{1 - \Gamma(p)}. \tag{A16}$$

The characteristic impedance of the first section $Z_{01} = Z_{01}(n, \epsilon, \mu, \nu)$ is obtained [27] via Richard's theorem as the value of $Z_d(p)$ at $p = 1$:

$$Z_{01} = Z_d(1). \tag{A17}$$

The function $Z_{01}(n, \epsilon, \mu, \nu)$ occupies a singular place in our design process because it is needed to find the required value of the parameter $\mu$ from Eq. (A23) or (A24).

The characteristic impedances $Z_{0k} = Z_{0k}(n, \epsilon, \mu, \nu)$ of the remaining sections $k = 2, 3, 4, \ldots, n$ of the cascade can be determined using the well-known subtraction technique [18]. Following [21], we have combined it with the transformation of the synthesis variable $p$ in order to improve accuracy of the extraction process. Such algorithms have been described by numerous authors and implemented in many computer codes and software tools; consequently, we omit the details here, but refer to the just cited papers.

**A6.** As well-known [27, 37, 22, Ch. 6], the sequence

$$r_G, Z_{01}, Z_{02}, Z_{03}, \ldots, Z_{0n}, r_L \tag{A18}$$

is strictly increasing or decreasing, depending on whether $\nu = 1$ or $\nu = -1$, respectively. Let us consider the individual VSWRs of the junctions of the prototype network. For the $k$-th junction in Fig. 1, we have:

$$V_k = \left( \frac{Z_{0k}}{Z_{0,k-1}} \right)^{\nu} \quad (k = 1, 2, 3, \ldots, n + 1) \tag{A19}$$

where the following notation is used:

$$Z_{00} = r_G, \quad Z_{0,n+1} = r_L. \tag{A20}$$

By considering the reverse operated transformer, it is easy to prove the well-known fact [37, 22, Sec. 6.02] that the functions

$$V_k = V_k(n, \epsilon, \mu), \quad (k = 1, 2, 3, \ldots, n + 1) \tag{A21}$$

do *not* depend upon the sign variable $\nu$. In other words, for given values of $n, \epsilon$ and $\mu$, the sequence of the VSWR values

$$V_1, V_2, V_3, \ldots V_{n+1} \tag{A22}$$

is the same for $\nu = 1$ and $\nu = -1$.

**A7.** Formula (A16) is used to find, for given $n$, $\epsilon$, $\nu$, and $r_G$, the value of $\mu$ which produces the required value $Z_{01,req}$ of characteristic impedance of the first section, or, equivalently, the VSWR $V_{1,req}$ for the first junction. This is done numerically by solving the equation

$$Z_{01}(n, \epsilon, \mu, \nu) = Z_{01,req}, \tag{A23}$$

or the equivalent equation

$$V_1(n, \epsilon, \mu) = V_{1,req} \tag{A24}$$

for the unknown $\mu$ on the interval $0 < \mu < 1$. This particular $\mu$ will be indicated by $\mu_0$. It follows from Eq. (A23) that $\mu_0 = \mu_0(n, \epsilon)$ does not depend upon the sign parameter $\nu$. Consequently, the fractional bandwidth $w_{q0}$ which is related to $\mu_0$ via Eq. (A4) is the *same* for $\nu = 1$ and $\nu = -1$.

Numerical experiments show that $Z_{01}(n, \epsilon, \mu, \nu)$ is a strictly monotonic function of $\mu$ which makes solving Eqs. (A23) and (A24) reasonably straightforward. It can also be seen that the fractional bandwidth $w_{q0}$ increases if one increases $n$ or reduces the $RL$ value.

**A8.** To illustrate the use of the synthesis procedure just described, we now calculate the realization parameters of transformer prototypes for the passband return loss $RL = 30\,\text{dB}$ ($\epsilon = 0.03164$) and the following four sample values of the VSWR for junction 1: $V_{1,req} = 12.1697$, 9.0892, 7.7347, and 5.0979. The considered specifications come about as a starting point in the design of matched waveguide applicators described in Section 3. The resulting design parameters are summarized in Tables A1 and A2.

**Table A1.** Specification of transformer prototypes of order $n = 1, 2, 3$, used in the design of open-ended or Teflon-sealed waveguide WR137 applicators for the frequency $f_0 = 7\,\text{GHz}$, and the arm tissue.

| Order | Waveguide without Teflon slab | | | | | | Waveguide with Teflon slab | | | | | |
|---|---|---|---|---|---|---|---|---|---|---|---|---|
| | $V_{1,req}$ | $V_{2,req}$ | $V_{3,req}$ | $V_{4,req}$ | $w_{30}$, % | $w_{21}$, % | $V_{1,req}$ | $V_{2,req}$ | $V_{3,req}$ | $V_{4,req}$ | $w_{30}$, % | $w_{21}$, % |
| $n = 1$ | 12.17 | 12.17 | n/a | n/a | 0.41 | 1.2 | 7.735 | 7.735 | n/a | n/a | 0.66 | 1.9 |
| $n = 2$ | 12.17 | 139.0 | 12.17 | n/a | 2.4 | 3.3 | 7.735 | 56.16 | 7.735 | n/a | 3.7 | 5.1 |
| $n = 3$ | 12.17 | 242.4 | 242.4 | 12.17 | 3.5 | 4.1 | 7.735 | 97.14 | 97.14 | 7.735 | 5.5 | 6.4 |

**Table A2.** Specification of transformer prototypes of order $n = 1, 2, 3$ used in the design of open-ended or Teflon-sealed waveguide WR137 applicators for the frequency $f_0 = 7\,\text{GHz}$, and the thigh tissue.

| Order | Waveguide without Teflon slab | | | | | | Waveguide with Teflon slab | | | | | |
|---|---|---|---|---|---|---|---|---|---|---|---|---|
| | $V_{1,req}$ | $V_{2,req}$ | $V_{3,req}$ | $V_{4,req}$ | $w_{30}$, % | $w_{21}$, % | $V_{1,req}$ | $V_{2,req}$ | $V_{3,req}$ | $V_{4,req}$ | $w_{30}$, % | $w_{21}$, % |
| $n = 1$ | 9.089 | 9.089 | n/a | n/a | 0.56 | 1.6 | 5.098 | 5.098 | n/a | n/a | 1.0 | 2.9 |
| $n = 2$ | 9.089 | 77.55 | 9.089 | n/a | 3.2 | 4.4 | 5.098 | 24.40 | 5.098 | n/a | 5.6 | 7.8 |
| $n = 3$ | 9.089 | 134.7 | 134.7 | 9.089 | 4.7 | 5.5 | 5.098 | 41.47 | 41.47 | 5.098 | 8.4 | 9.8 |

The VSWR values $V_{1,req} = 12.1697$ and 9.0892 ($V_{1,req} = 7.7347$ and 5.097) describe reflection from the load at $f_0 = 7\,\text{GHz}$ in the *hollow* (alternatively, *Teflon-sealed*) waveguide WR137 which is attached to the arm and thigh tissues, respectively, as shown in the right panel of Fig. 2. The parameters of Teflon slab and tissues are given in Section 3. As mentioned in the main body of the paper, the quantity $V_{1,req}$ can be determined either theoretically using an EM simulation software, or experimentally using a VNA; we calculated it in HFSS.

Given the larger bandwidth $w_{21}$ of the prototype transformers related to the waveguide with the Teflon-sealed end, we choose this structure for the implementation of matched waveguide applicators.

## APPENDIX B. EQUIVALENT NETWORKS

In this appendix, we formulate the conditions required to achieve equivalence (at a *single* frequency) of the scattering behavior of certain networks. These conditions are used in our design process to develop a matching circuit whose reflection properties in the presence of an absorbing load approximate those of the prototype transformer over the operating frequencies. It seems likely that similar conditions have already been suggested or implemented, but we did not find them published in the literature.

**B1.** Fig. B1(a) shows the network $N$ connected to two semi-infinite uniform lossless TLs of characteristic impedances $Z_{0a}$, $Z_{0b}$. This network is characterized by the scattering matrix[‡] $\underline{\underline{S}}$ as seen at Ports A and B. Let us confine ourselves to the case where the network $N$ is lossless and reciprocal. The scattering matrix of such a network is symmetric and unitary [6, Secs. 5.15, 5.16].

[‡] In this paper, we are dealing with the scattering matrices normalized to the characteristic impedances at each port. As is well known [6, Sec3. 5.13, 5.14], the characteristic impedance of the waveguide can always be made equal to 1 by normalizing the waveguide mode to 0.5 W of time-average power flow.

As a consequence, $\underline{\underline{S}}$ is shown to have the following general form employing concepts of [6, Eqs. (92), (99)] or [22, Eqs. (2.12-5), (2.12-9)] (indication of the frequency variable $f$ is suppressed):

$$\underline{\underline{S}} = \begin{bmatrix} Re^{j\theta_{aa}} & Te^{j\theta_{ab}} \\ Te^{j\theta_{ab}} & Re^{j\theta_{bb}} \end{bmatrix}. \tag{B1}$$

In this representation

$$R = \frac{V-1}{V+1}, \quad T = \frac{2\sqrt{V}}{V+1} \tag{B2}$$

are the linear magnitudes of scattering coefficients; $V$ $(1 < V < +\infty)$ is the VSWR at Port A (which is equal to that at Port B); and the phases $\theta_{aa}$, $\theta_{bb}$, and $\theta_{ab}$ of the scattering coefficients are constrained by the relation

$$e^{j2\pi m} = 1, \tag{B3}$$

where

$$m = \frac{1}{\pi}\left(\theta_{ab} - \frac{\theta_{aa}+\theta_{bb}}{2}\right) - \frac{1}{2}. \tag{B4}$$

By Eq. (B3), the parameter $m$ turns out to be an integer.

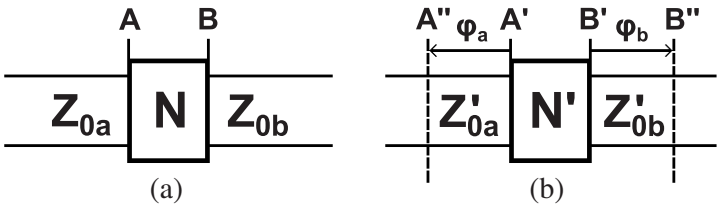


**Figure B1.** General two-port networks $N$, $N'$, and reference planes.

Let us introduce in Fig. B1(b) a different network $N'$, lossless and reciprocal, which is connected to two semi-infinite uniform lossless TLs of characteristic impedances $Z'_{0a}$, $Z'_{0b}$. This network is characterized by the scattering matrix $\underline{\underline{S}}'$ as seen at Ports $A'$ and $B'$. In a similar way to matrix $\underline{\underline{S}}$, we can derive the following general representation for $\underline{\underline{S}}'$:

$$\underline{\underline{S}}' = \begin{bmatrix} R'e^{j\theta'_{aa}} & T'e^{j\theta'_{ab}} \\ T'e^{j\theta'_{ab}} & R'e^{j\theta'_{bb}} \end{bmatrix}, \tag{B5}$$

where

$$R' = \frac{V'-1}{V'+1}, \quad T' = \frac{2\sqrt{V'}}{V'+1}, \tag{B6}$$

$V'$ is the VSWR at Ports $A', B'$ $(1 < V' < +\infty)$. The lossless reciprocity assumption imposes the following constraint on the phases $\theta'_{aa}$, $\theta'_{bb}$, $\theta'_{ab}$:

$$e^{j2\pi m'} = 1, \tag{B7}$$

with $m'$ defined as

$$m' = \frac{1}{\pi}\left(\theta'_{ab} - \frac{\theta'_{aa}+\theta'_{bb}}{2}\right) - \frac{1}{2}. \tag{B8}$$

According to (B7), the parameter $m'$ is always an integer. We shall view the parameters $m$, $m'$ as fixed values associated the networks $N$ and $N'$, respectively.

Two reference planes $A''$ and $B''$ are assumed in Fig. B1(b) at the electrical distances $\phi_a$, $\phi_b$ (either or both of which may be negative) from the corresponding Ports $A'$, $B'$ of network $N'$. When does the resulting network $N''$ defined between the reference planes $A''$ and $B''$ have, at a *fixed* frequency $f$, the same scattering matrix as that of network $N$?

One way to obtain the answer is to use the equivalent circuits of waveguide inhomogeneities. For example, a lossless reciprocal network may be always represented, at a given frequency, as either an ideal transformer [35] or impedance inverter [36, p. 166, 19] that are preceded and followed by appropriate lengths of TLs. The equivalent circuit elements and the location of the associated reference planes are usually expressed in terms of elements of the $Y$, $Z$ or chain matrix of the network.

Our answer to this question obviates the need for the equivalent circuit description of waveguide inhomogeneities. It is given by simple expressions (B16)–(B19) used to determine the required positions of the reference planes $A''$ and $B''$ directly in terms of the phases of scattering coefficients of the obstacles. The usefulness of our solution becomes apparent when converting the prototype transformer to a waveguide design by replacing the impedance steps by appropriate waveguide inhomogeneities. Our solution permits an easy determination of the separation between the obstacles in a waveguide through the phases of their scattering coefficients via Eq. (12). The aforementioned scattering coefficients can be readily obtained with the help of available EM simulation softwares.

**B2.** The scattering matrix of network $N''$ is [6, Sec. 5.17]

$$\underline{\underline{S}}'' = \begin{bmatrix} e^{-j\varphi_a} & 0 \\ 0 & e^{-j\varphi_b} \end{bmatrix} \cdot \underline{\underline{S}}' \cdot \begin{bmatrix} e^{-j\varphi_a} & 0 \\ 0 & e^{-j\varphi_b} \end{bmatrix}. \tag{B9}$$

By forcing (B9) to the form (B5) we obtain an obvious requirement that the VSWR values for both networks be the same:

$$V' = V, \tag{B10}$$

and arrive at the following system of equations for $\phi_a$, $\phi_b$:

$$e^{j(\theta'_{aa}-2\varphi_a)} = e^{j\theta_{aa}}, \tag{B11}$$

$$e^{j\left(\theta'_{bb}-2\varphi_b\right)} = e^{j\theta_{bb}}, \tag{B12}$$

$$e^{j\left(\theta'_{ab}-\varphi_a-\varphi_b\right)} = e^{j\theta_{ab}}. \tag{B13}$$

The general solution to the first two equations is given by

$$\varphi_a = \frac{\theta'_{aa}-\theta_{aa}}{2} + \pi n_a, \tag{B14}$$

$$\varphi_b = \frac{\theta'_{bb}-\theta_{bb}}{2} + \pi n_b, \tag{B15}$$

where $n_a, n_b = 0, \pm1, \pm2, \ldots$ are arbitrary integers. Inserting these expressions for $\phi_a$, $\phi_b$ into (B13) and taking the definitions (B4), (B8) into account, we get a constraint on $n_a, n_b$ that $n_1 + n_2 + m - m'$ is an *even* integer (recall that by (B3) and (B7), the parameters $m$, $m'$ are integer values). Based on this, we can eliminate $n_b$ or $n_a$ and write the solution to Eqs. (B11)–(B13) as

$$\varphi_a = \frac{\theta'_{aa}-\theta_{aa}}{2} + \pi n_a, \tag{B16}$$

$$\varphi_b = \frac{\theta'_{bb}-\theta_{bb}}{2} + \pi(m'-m) - \pi n_a + 2\pi n, \tag{B17}$$

or, equivalently,

$$\varphi_a = \frac{\theta'_{aa}-\theta_{aa}}{2} + \pi(m'-m) - \pi n_b + 2\pi n, \tag{B18}$$

$$\varphi_b = \frac{\theta'_{bb}-\theta_{bb}}{2} + \pi n_b, \tag{B19}$$

where $n_a$, $n_b$ are the same as before, and $n = 0, \pm1, \pm2, \ldots$ is an arbitrary integer value.

When the network $N$ is a junction of the TLs involved, and the reference planes 1 and 2 are located at the junction, the appertaining scattering matrix assumes the form

$$\underline{\underline{S}} = \frac{1}{Z_{0a}+Z_{0b}} \begin{pmatrix} Z_{0b}-Z_{0a} & 2\sqrt{Z_{0a}Z_{0b}} \\ 2\sqrt{Z_{0a}Z_{0b}} & Z_{0a}-Z_{0b} \end{pmatrix}. \tag{B20}$$

It can be easily seen that for $Z_{0a} < Z_{0b}$

$$V = \frac{Z_{0b}}{Z_{0a}}, \quad \theta_{aa} = 0, \quad \theta_{bb} = \pi, \quad \theta_{ab} = 0, \quad m = -1, \tag{B21}$$

and for $Z_{0a} > Z_{0b}$

$$V = \frac{Z_{0a}}{Z_{0b}}, \quad \theta_{aa} = \pi, \quad \theta_{bb} = 0, \quad \theta_{ab} = 0, \quad m = -1. \tag{B22}$$

We apply the above theory to realize the matched applicator in waveguide technology by replacing the impedance steps $2, 3, 4, \ldots, n+1$ (networks $N$ in our nomenclature) of the prototype transformer by the obstacles (networks $N'$) which are distributed along the waveguide and which, together with the waveguide sections of positive or negative electrical lengths $\varphi_a$, $\varphi_b$ (networks $N''$), have the same scattering matrix $\underline{\underline{S}}''$ as the respective impedance steps, at the synchronous frequency $f_s$. According to Eqs. (B16)–(B19), there is an infinite number of electrical lengths $\phi_a$, $\phi_b$ for each obstacle.

**B3.** In the second equivalence problem, the solution used in the design procedure is illustrated in Fig. B2. Its analysis is obvious, but it was deemed useful to describe it for easy reference.


**Figure B2.** General one-port networks $N$, $N'$, and reference planes.

The one-port networks $N$ and $N'$ are characterized by the scattering (reflection) coefficients $S$ and $S'$ at the reference planes $B$ and $B'$, respectively. (The EM waves are incident from and reflected to the right of the networks.) We parameterize these scattering coefficients by the VSWR values $V, V'$ and phases $\theta_{bb}$, $\theta'_{bb}$ as

$$S = \frac{V-1}{V+1} e^{j\theta_{bb}}, \tag{B23}$$

$$S' = \frac{V'-1}{V'+1} e^{j\theta'_{bb}}. \tag{B24}$$

The network $N''$ is obtained from the network $N'$, by moving the reference plane away from $B'$ by the electrical distance $\varphi_b$, as shown in the right panel of Fig. B2. The appertaining scattering coefficient $S''$ at the reference plane $B''$ is [6, Sec. 5.17]

$$S'' = e^{-2j\varphi_b} S'. \tag{B25}$$

When does the networks $N$ and $N''$ have the same scattering coefficients? (We remind the reader that this question is formulated for a fixed frequency.)

The answer is obtained by the comparison of Eq. (B25) with (B23) and is undoubtedly well known: the VSWRs for the networks $N$ and $N'$ must be the same ($V = V'$) and

$$\varphi_b = \frac{\theta'_{bb} - \theta_{bb}}{2} + \pi n_b, \tag{B26}$$

where $n_b = 0, \pm 1, \pm 2, \ldots$ is an arbitrary integer.

In our design method, the network $N$ describes the junction of the prototype transformer labeled as number 1 in Fig. 1. It is regarded here as a one port network which consists of the TL of characteristic impedance $Z_{0b} = Z_{01}$ terminated in the TL of characteristic impedance $r_G$, with the reference plane $B$ located at the junction. The corresponding scattering coefficient

$$S = \frac{r_G - Z_{01}}{r_G + Z_{01}} \tag{B27}$$

is real and characterized by the phase

$$\theta_{bb} = \begin{cases} \pi & Z_{01} > r_G \\ 0 & Z_{01} < r_G \end{cases} \tag{B28}$$

according to whether the sign parameter $\nu$ from Appendix A is set to 1 or $-1$. By Eq. (A21), the appertaining VSWR $V = V_1(n, \epsilon, \mu)$ is a function of the number of sections $n$ and the parameters $\epsilon, \mu$, and does not depend upon $\nu$.

In the same framework, the network $N'$ represents, at the synchronous frequency $f_s$, the reflection behavior of the *unmatched* waveguide that is stationed in the same position relative to the tissue as the matched applicator under design. The precise location of the reference plane $B'$ is described in the main text. The modal reflection coefficient $S'$ is assumed to be available from measurements or numerical modeling, hence the quantities $V'$ and $\theta'_{bb}$ are viewed as given values.

In the design process, we make the networks $N$ and $N''$ equivalent (in our sense) at the synchronous frequency $f_s$ by choosing the synthesis parameter $\mu$ to satisfy Eq. (A23) or, alternatively, employing Eq. (A24) with $V_{1,req} = V'$, and selecting the electrical distance $\varphi_b$ at $f_s$ along the waveguide, in accordance with Eq. (B26). Note that we have a infinite number of solutions for $\varphi_b$.

## REFERENCES


1. AbuHussain, M. and U. C. Hasar, "Design of X-bandpass waveguide Chebyshev filter based on CSRR metamaterial for telecommunication systems," *Electronics (Basel)*, Vol. 9, No. 1, article 101, Jan. 2020.
2. Asan, N. B., E. Hassan, J. Velander, S. R. M. Shah, D. Noreland, T. J. Blokhius, E. Wadbro, M. Berggren, T. Voigt, and R. Augustine, "Characterization of the fat channel for intra-body communication at R-band frequencies," *Sensors (Basel)*, Vol. 18, No. 9, article 2752, Sep. 2018.
3. Bertin, E., N. Crespi, and T. Magedanz, Eds., *Shaping Future 6G Networks. Needs, Impacts, and Technologies*, Wiley, Hoboken, NJ, 2022.
4. Cohn, S. B., "Design of simple broad-band wave-guide-to-coaxial-line junctions," *Proc. IRE*, Vol. 35, No. 9, 920–926, Sep. 1947.
5. Dakhov, V. M., V. A. Katrich, and M. V. Nesterenko, "Compact radiator for microwave hyperthermia," *Microwave & Telecommunication Technology (CriMiCo2008), 18th Int. Crimean Conf.*, 860–861, Sevastopol, Crimea, Ukraine, Sep. 08–12, 2008.
6. Dicke, R. H., "General microwave circuit theorems," *Principles of Microwave Circuits*, 130–161, Montgomery, C. G., R. H. Dicke, and E. M. Purcell, Eds., McGraw-Hill, New York, NY, 1948.
7. Dishal, M., "Alignment and adjustment of synchronously tuned multiple-resonant-circuit filters," *Proc. IRE*, Vol. 39, No. 11, 1148–1455, Nov. 1951.
8. Eskelinen, H. and P. Eskelinen, *Microwave Component Mechanics*, Artech House, Boston, MA, 2003.
9. Gajda, G. B., E. Lemay, and J. Paradis, "Model of steady-state temperature rise in multilayer tissues due to narrow-beam millimeter-wave radiofrequency field exposure," *Health Phys.*, Vol. 117, No. 3, 254–266, Mar. 2019.
10. Gupta, R. and S. Singh, "Development and analysis of a microwave direct contact water-loaded box-horn applicator for therapeutic heating of bio-medium," *Progress In Electromagnetics Research*, Vol. 62, 217–235, 2006.
11. International Commission on Non-Ionizing Radiation Protection (ICNIRP), "Guidelines for limiting exposure to electromagnetic fields (100 kHz to 300 GHz), *Health Phys.*, Vol. 118, No. 5, 483–524, May 2020.
12. Kantor, G. and D. M. Witters, "The performance of a new 915-MHz direct contact applicator with reduced leakage," *J. Microw. Power*, Vol. 18, No. 2, 133–142, Jun. 1983.
13. Keshavarz, S., R. Keshavarz, and A. Abdipour, "Compact active duplexer based on CSRR and interdigital loaded microstrip coupled lines for LTE application," *Progress In Electromagnetics Research C*, Vol. 109, 27–37, 2021.

14. Khan, S. R., S. K. Pavuluri, G. Cummins, and M. P. Y. Desmulliez, "Wireless power transfer techniques for implantable medical devices: A review," *Sensors (Basel)*, Vol. 20, No. 12, article 3487, Jun. 2020.
15. Lakhtakia, A. and T. G. Mackay, "Meet the metamaterals," *Opt. Photonics News*, Vol. 18, No. 1, 32–39, Jan. 2007.
16. Lee, Y. and K. Hwang, "Skin thickness of Korean adults," *Surg. Radiol. Anat.*, Vol. 24, Nos. 3–4, 183–189, Aug.–Sep. 2002.
17. Lemay, E., G. B. Gajda, G. W. McGarr, M. Zhuk, and J. Paradis, "Analysis of ICNIRP 2020 basic restrictions for localized radiofrequency exposure in the frequency range above 6 GHz," *Health Phys.*, Vol. 123, No. 3, 179–196, Sep. 2022.
18. Levy, R., "Tables of element values for the distributed low-pass prototype filter," *IEEE Trans. Microw. Theory Techn.*, Vol. 13, No. 5, 514–536, Sep. 1965.
19. Levy, R., "A generalized design technique for practical distributed reciprocal ladder networks," *IEEE Trans. Microw. Theory Techn.*, Vol. 21, No. 8, 519–526, Aug. 1973.
20. Levy, R. and L. W. Hendrick, "Analysis and synthesis of in-line coaxial-to-waveguide adapters," *2002 IEEE MTT–S Int. Microw. Symp. Dig.*, 809–811, Seattle, WA, USA, Jun. 02–07, 2002.
21. Lind, L. F., "Synthesis of equally terminated low-pass lumped and distributed filters of even order," *IEEE Trans. Microw. Theory Techn.*, Vol. 17, No. 1, 43–45, Jan. 1969.
22. Matthaei, G. L., L. Young, and E. M. T. Jones, *Microwave Filters, Impedance-Matching Networks, and Coupling Structures*, Artech House, Norwood, MA, 1980.
23. Mehdizadeh, M., "Microwave/RF applicators and probes for material heating, sensing and plasma generation. A design guide," 2nd Edition, Elsevier, Oxford, UK, 2010.
24. Ness, J. B., "A unified approach to the design, measurement, and tuning of coupled resonator filters," *IEEE Trans. Microw. Theory Techn.*, Vol. 46, No. 4, 343–351, Apr. 1998.
25. Pokharel, R. K., A. Barakat, S. Alshhawy, K. Yoshitomi, and C. Sarris, "Wireless power transfer system rigid to tissue characteristics using metamaterial inspired geometry for biomedical implant applications," *Sci. Rep.*, Vol. 11, article 5868, Mar. 12, 2021.
26. Rappaport, C., "Synthesis of optimum microwave antenna applicators for use in treating deep localized tumors," *Progress In Electromagnetics Research*, Vol. 1, 175–240, 1989.
27. Riblet, H. J., "General synthesis of quarter-wave impedance transformers," *IRE Trans. Microw. Theory Techn.*, Vol. 5, No. 1, 36–43, Jan. 1957.
28. Sasaki, K., K. Wake, and S. Watanabe, "Measurement of the dielectric properties of the epidermis and dermis at frequencies from 0.5 GHz to 110 GHz," *Phys. Med. Biol.*, Vol. 59, No. 16, 4739–4747, Aug. 21, 2014.
29. Sasaki, K., M. Mizuno, K. Wake, and S. Watanabe, "Monte Carlo simulations of skin exposure to electromagnetic field from 10 GHz to 1 THz," *Phys. Med. Biol.*, Vol. 62, No. 17, 6993–7010, Aug. 09, 2017.
30. Stutzman, W. L. and G. A. Thiele, *Antenna Theory and Design*, 3rd Edition, Wiley, 2013.
31. Uher, J., J. Bornemann, and U. Rosenberg, *Microwave Components for Antenna Feed Systems: Theory and CAD*, Artech House, Norwood, MA, 1993.
32. Vrba, D., D. Rodrigues, J. Vrba, and P. R. Stauffer, "Metamaterial antenna arrays for improved uniformity of microwave hyperthermia treatments," *Progress In Electromagnetics Research*, Vol. 156, 1–12, 2016.
33. Wang, Q. and J. Bornemann, "Synthesis and design of direct-coupled rectangular waveguide filters with arbitrary inverter sequence," *2014 16th Int. Symp. Antenna Technol. Appl. Electromagnetics (ANTEM)*, 1–6, Victoria, BC, Canada, Jul. 13–16, 2014.
34. Wang, Y., F. Qi, Z. Liu, P. Liu, W. Li, H. Wu, and W. Ning, "A wideband method to enhance the terahertz prenetration in human skin based on a 3D printed dielectric rod waveguide," *IEEE Trans. Terahertz Sci. Technol.*, Vol. 9, No. 2, 155–164, Mar. 2019.

35. Weißfloch, A., "Anwendung des Transformationssatzes über verlustlose Vierpole auf die Hintereinanderschaltung von Vierpolen," *Hochfrequenztechn. u. Elektroakust.*, Vol. 61, No. 1, 19–28, Jan. 1943.
36. Weissfloch, A., *Schaltungstheorie und Messtechnik des Dezimeter- und Zentimeter-Wellengebietes*, Birkhäuser, Basel, Switzerland, 1954.
37. Young, L., "The quarter-wave transformer prototype circuit," *IRE Trans. Microw. Theory Techn.*, Vol. 8, No. 5, 483–489, Sep. 1960.
38. Yu, M. and Y. Wang, "Synthesis and beyond," *IEEE Microw. Mag.*, Vol. 12, No. 6, 63–76, Oct. 2011.
39. Zoughi, R., *Microwave Non-Destructive Testing and Evaluation*, Kluwer, London, UK, 2000.